

Training Deep Learning Models for Massive MIMO CSI Feedback with Small Datasets in New Environments

Zhenyu Liu, *Member, IEEE*, and Zhi Ding, *Fellow, IEEE*

Abstract

Deep learning (DL)-based channel state information (CSI) feedback has shown promising potential to improve spectrum efficiency in massive MIMO systems. However, practical DL approaches require a sizeable CSI dataset for each scenario, and require large storage for multiple learned models. To overcome this costly barrier, we develop a solution for efficient training and deployment enhancement of DL-based CSI feedback by exploiting a lightweight translation model to cope with new CSI environments and by proposing novel dataset augmentation based on domain knowledge. Specifically, we first develop a deep unfolding CSI feedback network, SPTM2-ISTANet+, which employs spherical normalization to address the challenge of path loss variation. We also introduce an integration of a trainable measurement matrix and residual CSI recovery blocks within SPTM2-ISTANet+ to improve efficiency and accuracy. Using SPTM2-ISTANet+ as the anchor feedback model, we propose an efficient scenario-adaptive CSI feedback architecture. This new CSI-TransNet exploits a plug-in module for CSI translation consisting of a sparsity aligning function and lightweight DL module to reuse pretrained models in unseen environments. To work with small datasets, we propose a lightweight and general augmentation strategy based on domain knowledge. Test results demonstrate the efficacy and efficiency of the proposed solution for accurate CSI feedback given limited measurements for unseen CSI environments.

Index Terms

Massive MIMO, CSI feedback, CSI augmentation, deep learning, multi-scenario

Z. Liu is with the School of Computer Science (National Pilot Software Engineering School), Beijing University of Posts and Telecommunications, China (e-mail: lzyu@bupt.edu.cn).

Z. Ding is with the Department of Electrical and Computer Engineering, University of California at Davis, USA (e-mail: zding@ucdavis.edu).

I. INTRODUCTION

Modern wireless communication systems have made tremendous strides in utilizing the spatial diversity afforded by multiple-input multiple-output (MIMO) transceivers to improve radio link performance. In particular, massive MIMO systems have shown great promise for delivering high spectrum and energy efficiency for 5G wireless systems and beyond. The efficiency of massive MIMO downlink depends on accurate downlink CSI estimates at gNodeB (gNB) for transmission precoding. For massive MIMO systems, such feedback data can be substantial because of the large number of antennas and wide bandwidth. This challenge strongly motivates many research efforts aimed at accurate downlink CSI feedback in frequency division duplex (FDD) systems.

Compressive sensing (CS) approaches can exploit channel properties including low rank or sparsity in spatial [1] or temporal domain [2] to reduce the bandwidth for CSI feedback. However, CS approaches rely on the strong sparsity condition which may not strictly hold and can limit their efficacy [3]. A number of recent works have explored deep neural networks (DNN) for downlink CSI compression and feedback. Deep learning (DL) based CSI feedback has shown good recovery accuracy and time efficiency by exploiting characteristics such as spatial and spectral coherence [3], [4], [5], [6], [7], bi-directional reciprocity [8], [9], and temporal correlation [10], [11], [12]. However, DL training requires a large number of channel measurements for each customized model. Collecting these CSI measurements can be labor-intensive and quite costly. Furthermore, a single CSI model tends to exhibit poor performance when applied to other radio-frequency (RF) environments due to model mismatch. Training multiple parallel DL models would further incur higher training cost, computation complexity and storage space to deploy.

Another major challenge lies in the need for sufficient training data from real-time channel measurements that underlie DL solutions. Effectively augmenting a small set of measurement data for DL training can substantially reduce the cost of labor-intensive measurement and mitigate model overfitting [13]. However, traditional data augmentation techniques commonly used in image processing such as geometric transformation, cropping, or rotation are incompatible with physical radio channels. To our best knowledge, CSI data augmentation has not been explored and requires domain knowledge of radio propagation physics. Another direction applies generative adversarial network (GAN) as a blackbox for CSI augmentation [14], [15], [16]. Ironically, blackbox GAN itself often requires training with a large number of CSI measurements. Moreover, GAN designed for massive MIMO [16] can be computationally costly and may require billions

of floating point operations (FLOPs).

In addition to data augmentation, to improve CSI recovery accuracy from limited available data samples, DNN should be capable of handling complex CSI features and variations. Generally, existing DL-based CSI feedback works [5], [7], [8] have demonstrated substantially better performance against indoor channels but tend to be less effective for the more complex outdoor channels. Furthermore, CSI from wide bandwidth and massive antennas tend to exhibit a high degree of variation. Path loss alone can vary the CSI magnitude by several orders. Such inherent CSI characteristics can be particularly troublesome for DL-based CSI compression and feedback system trained with only a small dataset of measured CSIs that lack broad representation. Thus, the ability to process massive MIMO CSI from a wide variety of deployment scenarios is a difficult challenge in the practical deployment of DL-based CSI feedback schemes. We propose a new training regime based on the transfer learning principle.

The principle of transfer learning [17], [18] leverages cross-task correlations in different scenarios to reduce training cost. For the problem of CSI encoding and compression for feedback, user equipments (UEs) need sufficient memory to store encoder DNNs or to update parameters of the encoder DNN frequently, typically requiring large storage and/or transmission bandwidth for encoder networks, each with as many as millions of parameters [3], [4], [5], [6], [7]. A UE-friendly design of multi-task, learning-based CSI feedback has been proposed for the multiple CSI scenarios [19]. By exploiting a shared encoder and multiple task-specific decoders, the joint feedback architecture of [19] can lead to a considerable reduction of UE storage use. However, a shared encoder can degrade CSI recovery accuracy due to the lack of environment-specific features. Moreover, information in the pretrained model has not been fully exploited to facilitate practical implementation.

To design a scenario-adaptive and high-accuracy CSI feedback solution with limited CSI samples and deployment cost, we develop an efficient DL feedback architecture amenable to enhanced training and deployment despite a small training dataset. Our objectives are to improve the recovery accuracy and robustness of the CSI feedback network for suitable deployment in a variety of environments by developing a UE-friendly design in conjunction with simple data augmentation for training based on physical insights and domain knowledge. We design an optimized DL structure to process CSI samples with complex features. Starting with the pretrained model, we design plug-in modules consisting of the sparsity aligning and shallow convolutional neural network (CNN) to implement CSI translation across different channel

environments. We utilize physical insights and domain knowledge regarding radio channels to devise a lightweight UE encoder together with a simple but effective CSI data augmentation technique. Our contributions are summarized as follows:

- Practical deployment of existing DL-based CSI feedback mechanism can be hindered by insufficient channel measurements needed to train large-scale DNNs. Training multiple models against various radio environments further elevates the difficulty. In this paper, we design a scenario-adaptive CSI compression framework which requires few channel measurements for training and can reuse pretrained DL model in a new and possibly unseen environment. This framework is compatible with existing CSI feedback methods by only customizing and inserting a translation module and a retranslation module.
- We develop an efficient plug-in CSI feedback architecture that includes a translation module to process CSI data from a new RF environment to the known format used in pretraining, effectively reusing the pretrained CSI model with high recovery accuracy. By customizing an effective sparsity aligning function in angular-delay domain and a lightweight CNN model with only thousands of additional parameters, our proposed translation module can reuse the pretrained CSI network and achieve high recovery accuracy, instead of using a separate encoder network [3], [4], [5], [7] always requires millions of parameters. To our best knowledge, this is the first work proposing CSI translation to effectively generate feedback models.
- To improve CSI feedback efficiency and recovery accuracy in complex environments, we propose an efficient CSI feedback framework inspired by CS, named SPTM2-ISTANet+. This model uses a spherical feedback structure to regulate input distribution and mitigate the effect of path loss. Our deep unfolding decoder network with residual recovery structure improves CSI recovery accuracy, with which we construct a trainable encoder network to overcome shortcomings of a pre-set sparse transformation in CS and improve encoding efficiency. Simulation results demonstrate superior performance, including normalized mean square error (NMSE) of -24.3 dB at compression ratio (CR) of $1/4$ in a popular outdoor scenario [3].
- Instead of training a blackbox GAN to generate augmented CS samples, we develop a simple but effective model-driven augmentation strategy by exploiting domain knowledge and physical features of CSI matrices based on domain insight. Taking into consideration

of geographical continuity and delay property of MIMO channels, we develop a circular shifting augmentation of CSI magnitudes in angular-delay domain to incorporate the circular property of discrete Fourier transform (DFT). We also apply random phase variation to CSI elements to imitate channel phase changes and mitigate overfitting. Test results demonstrate significantly enhanced CSI recovery performance over blackbox GAN, and can achieve NMSE of -15.8 dB based on only 100 measurement samples at CR of $1/4$ in the outdoor scenario.

II. SYSTEM MODEL

Without loss of generality, we consider a massive MIMO gNB equipped with N_b antennas to serve a number of single-antenna UEs within its coverage. Orthogonal frequency division multiplexing (OFDM) is adopted in downlink transmission over N_f subcarriers. For subcarrier m , let $\mathbf{h}_m \in \mathbb{C}^{N_b \times 1}$ denote the channel vector, $\mathbf{w}_m \in \mathbb{C}^{N_b \times 1}$ denote transmit precoding vector, $x_m \in \mathbb{C}$ denote the transmitted data symbol, and $n_m \in \mathbb{C}$ denote the additive noise. Correspondingly, the received signal of the UE is

$$y_m = \mathbf{h}_m^H \mathbf{w}_m x_m + n_m, \quad (1)$$

where $(\cdot)^H$ represents the conjugate transpose. The downlink CSI matrix in the spatial-frequency domain is denoted by $\tilde{\mathbf{H}} = [\mathbf{h}_1, \dots, \mathbf{h}_{N_f}]^H \in \mathbb{C}^{N_f \times N_b}$.

To reduce feedback overhead, we first exploit the sparsity of CSI in the delay domain. Applying 2D DFT, CSI matrix \mathbf{H}_{sf} in spatial-frequency domain can be transformed to be \mathbf{H}_{ad} in angular-delay domain using

$$\mathbf{F}_d^H \mathbf{H}_{sf} \mathbf{F}_a = \mathbf{H}_{ad}, \quad (2)$$

where \mathbf{F}_d and \mathbf{F}_a denote the $N_f \times N_f$ and $N_b \times N_b$ unitary DFT matrices, respectively. Owing to limited delay spread and scatters in the practical radio environment, most elements in the $N_f \times N_b$ matrix \mathbf{H}_{ad} are negligibly small except for its first R_d rows [3]. Therefore, we can approximate the MIMO channel by keeping the first R_d rows of \mathbf{H}_{ad} , denoted by \mathbf{H} .

To allow DL-based CSI feedback system to track the space-varying characteristics of wireless fading channels under different environments, mobile network operators need to collect channel measurements in each environment and train a corresponding DL network. Furthermore, UEs entering a new environment would need to adjust their encoder DL network which may be large

with millions of parameters. Assuming T typical scenarios in a region, we can use \mathbf{H}^t to denote the channel matrix for scenario t .

We aim to reduce the amount of channel measurement data needed for training in new environments and to reduce the deployment cost of DL models for CSI feedback. In this paper, we construct a “few-shot” learning CSI framework from the following three perspectives:

- The DL framework for CSI feedback should achieve high-accuracy recovery under complex channel environments, which requires a powerful decoding network. On the other hand, the DL feedback model must cope with CSI variability.
- Data augmentation should help explore prominent MIMO channel features to lower the amount of required channel measurements, and cover cases that may be absent in measured data.
- DL feedback model should be able to leverage prior training outcomes from known channel environment to reduce training complexity and deployment cost.

To leverage prior training outcomes from a previously known scenario, we design our DL feedback networks for CSI feedback under changing scenarios in two phases: a) constructing a DL network in an anchor scenario without prior information ($t = 1$); b) constructing DL networks for additional scenarios ($t = 2, 3, \dots, T$) by leveraging the information learned in prior training phase a).

Let $\hat{\mathbf{H}}^t$ be the recovered CSI matrix by the decoder in scenario t corresponding to the ground-truth \mathbf{H}^t . Define the encoding and decoding function as $f_{\text{en}}(\cdot)$ and $f_{\text{de}}(\cdot)$, respectively. For downlink CSI feedback architecture in the anchor scenario, the encoder network and decoder network can be denoted, respectively, by

$$\mathbf{s}_1 = f_{\text{en},1}(\mathbf{H}^1; \Phi_1), \quad (3)$$

$$\hat{\mathbf{H}}^1 = f_{\text{de},1}(\mathbf{s}_1; \Psi_1). \quad (4)$$

For the subsequent scenario t ($t \geq 2$), the encoder network and decoder network can be formed, respectively, by

$$\mathbf{s}_t = f_{\text{en},t}(\mathbf{H}^t; \Phi_t | \Phi_1, \Psi_1), \quad (5)$$

$$\hat{\mathbf{H}}^t = f_{\text{de},t}(\mathbf{s}_t; \Psi_t | \Phi_1, \Psi_1). \quad (6)$$

Next, we construct a DL-based CSI feedback framework to reduce the deployment cost of DL models in variational environments and to improve CSI recovery by DL models trained with limited channel measurement data.

III. OVERALL FRAMEWORK

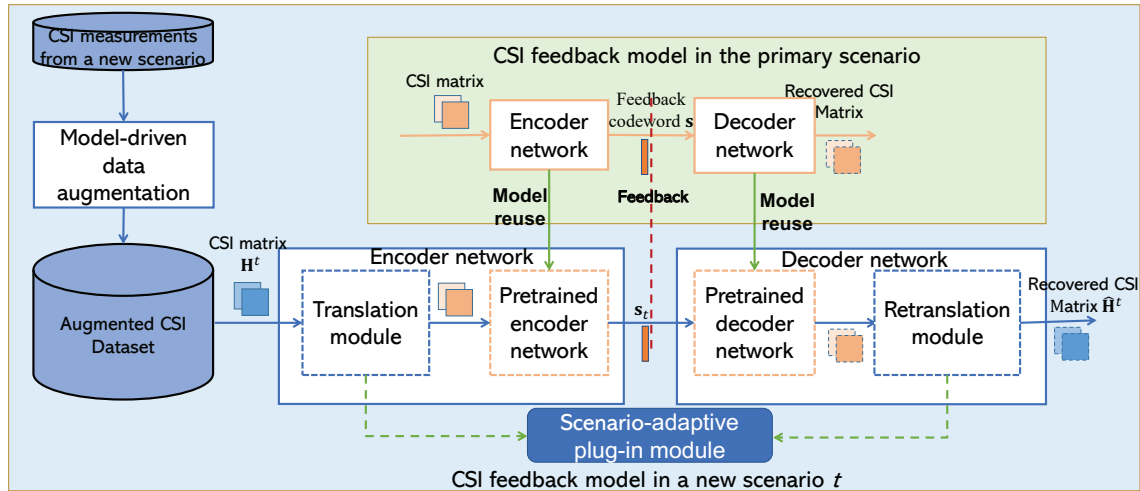


Fig. 1: Architecture of overall framework

DL networks for CSI feedback are generally optimized via training from CSI data samples for a customized radio propagation scenario. To cover a city with various scenario types, large numbers of channel measurements are often required for each likely scenario, and training cost can be high. First, retraining a new DL network for a new scenario would be costly. Storing trained encoder networks in anticipation of a large number of scenarios at UE would require large amount of memory particularly for many encoder models with millions of parameters [3], [4], [5], [6], [7]. To reduce the deployment cost of DL-based CSI feedback models, this work sets two anchor objectives: (1) to design a scenario-adaptive DL framework for accurate CSI recovery; (2) to develop efficient use of limited CSI data measurement in DL training based on domain knowledge.

To achieve these two objectives, we propose a scenario-adaptive CSI feedback framework that reuses pretrained high-accuracy CSI feedback model together with the model-driven data augmentation in new environments. As shown in Fig. 1, the overall framework consists of the following three modules:

- **A robust backbone model trained for an anchor scenario.** The key idea is to construct an accurate and robust backbone model which can be reused when facing new environments to reduce the deployment cost. However, CSI matrices of massive MIMO always exhibit a high degree of variation and suffer from feedback performance degradation as the CSI variation range expands [19]. Consequently, we construct an efficient compressive CSI feedback architecture, named SPTM2-ISTANet+, to accommodate complex CSI features and variations as the backbone network. SPTM2-ISTANet+ consists of a spherical feedback structure and a CS-inspired DNN model to enhance feedback robustness and accuracy. The detailed design of SPTM2-ISTANet+ is introduced in Section IV.
- **A scenario-adaptive plug-in module.** By translating CSI matrices in a new scenario into a “style” compatible with the anchor scenario during pre-training, the pretrained backbone network can be reused together with a lightweight deployment cost. Thus, we propose a lightweight plug-in module for scenario adaption that only consists of a few thousand trainable parameters to be updated against a new scenario. A translation module and a retranslation module are integrated to implement CSI style translation and recovery. The detailed design of the style translator is introduced in Section V.
- **A model-driven data augmentation module.** To reduce the cost associated with labor-intensive channel measurement, we customize a simple but effective model-driven augmentation module by exploiting physical features of CSI matrices based on domain knowledge. CSI magnitudes and phases are augmented separately in view of their correlative channel properties. The detailed design of model-driven data augmentation is explained in Section VI.

IV. SPTM2-ISTANET+

We now construct an efficient deep unfolding network as the backbone model for the anchor scenario to improve CSI feedback accuracy.

A. Encoding Network

To improve the robustness and CSI compression efficiency, we adopt a deep unfolding-based feedback network, and propose two key innovations to the encoder network in view of physical CSI features.

First, we construct a spherical CSI feedback structure in view of domain-specific characteristics of the wireless channel. The distribution of MIMO CSI coefficients is substantially different from

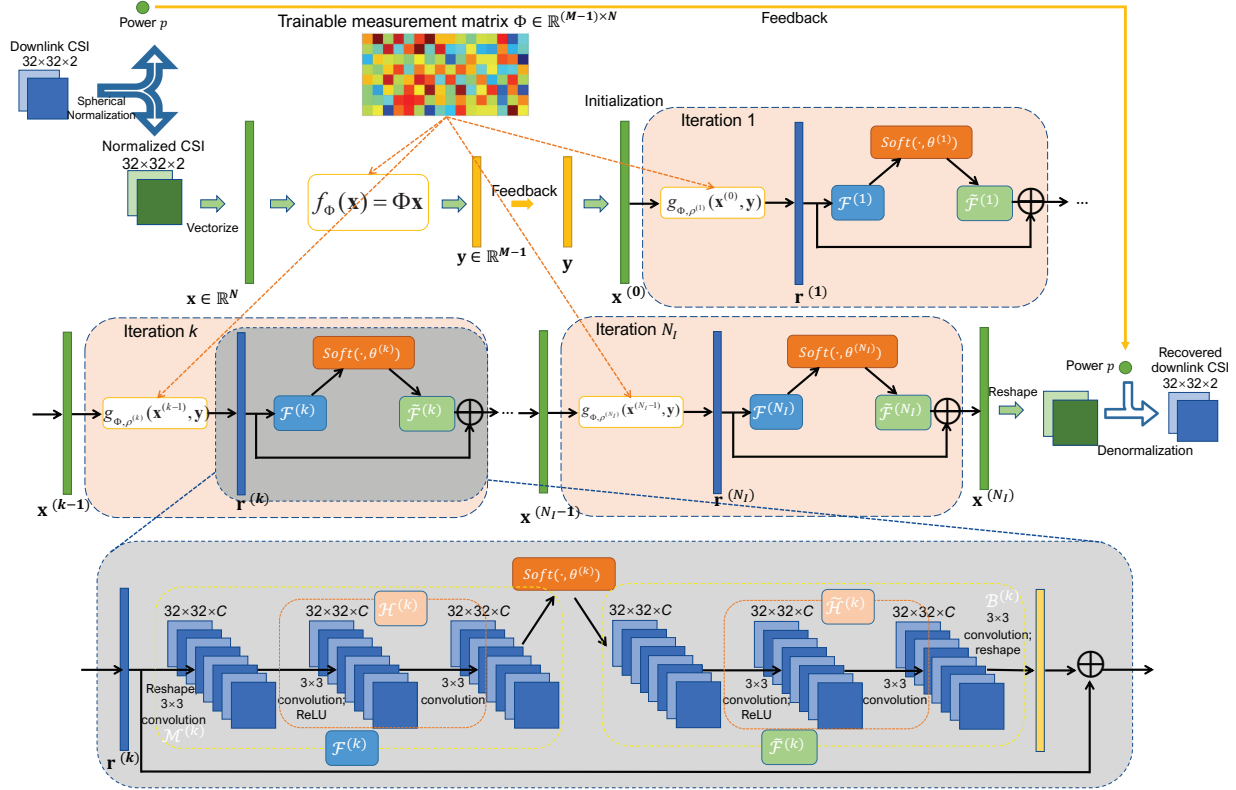


Fig. 2: Architecture of SPTM2-ISTANet+.

that of image data. The dynamic range of CSI is always much greater because of radio path loss, as CSI of one UE may differ from that of another by orders of magnitude. A naive processing can render CSI of some UE too small, leading to large recovery errors. Hence, before applying the CS measurement matrix to lower CSI dimensionality, we split CSI matrix \mathbf{H} into a power value p and a spherical matrix $\check{\mathbf{H}}$, where $p = \|\mathbf{H}\|$ is the power and $\check{\mathbf{H}} = \mathbf{H}/\|\mathbf{H}\|$ is a unit norm spherical CSI.

As shown in Fig. 2, after the spherical processing, we vectorize the normalized downlink CSI matrix $\check{\mathbf{H}}$ as the input to DNN for compression. The real part and imaginary part are split for easier processing. The corresponding vector is denoted as $\mathbf{x} \in \mathbb{R}^N$, where $N = 2 \times R_d \times N_b$. To shorten \mathbf{x} , a measurement matrix $\Phi \in \mathbb{R}^{(M-1) \times N}$ is used for dimension compression, where $M = CR \times N - 1$.

Second, to deliver further performance improvement, we move away from the traditional random constructed measurement matrix in CS and devise a data-driven trainable measurement matrix Φ . The goal is to better capture features of massive MIMO for CSI encoding, particularly if the compression degree is high (i.e. CR is small). Using only a matrix multiplication at the

encoder, UE computation cost is modest.

B. Decoding Network

Assuming lossless feedback [3], [20], the low-dimension vector $\mathbf{y} \in \mathbb{R}^{M-1}$ received by gNB can be defined as $\mathbf{y} = \Phi\mathbf{x}$. From \mathbf{y} , the decoder network reconstructs the original \mathbf{x} by solving the following compressive sensing recovery problem:

$$\min_{\mathbf{x}} \frac{1}{2} \|\Phi\mathbf{x} - \mathbf{y}\|^2 + \lambda \|\mathcal{F}(\mathbf{x})\|_1, \quad (7)$$

where λ is the regularization parameter, $\|\cdot\|$ denotes the l_2 -norm. $\mathcal{F}(\cdot)$ is the sparse transform function of \mathbf{x} .

Our decoder network of SPTM2-ISTANet+ utilizes the deep unfold structure. Adopting the settings of ISTANet+ [21] to unfold the iterative shrinkage-thresholding algorithm (ISTA) [22], we recover CSI by iterating between two steps:

$$\mathbf{r}^{(k)} = \mathbf{x}^{(k-1)} - \rho\Phi^\top (\Phi\mathbf{x}^{(k-1)} - \mathbf{y}), \quad (8)$$

$$\mathbf{x}^{(k)} = \arg \min_{\mathbf{x}} \frac{1}{2} \|\mathbf{x} - \mathbf{r}^{(k)}\|^2 + \lambda \|\mathcal{F}(\mathbf{x})\|_1, \quad (9)$$

where k denotes the iteration index, ρ denotes the step size. Next, we expand Eq. (8) and Eq. (9) respectively into deep unfolding modules corresponding to the k -th iteration, as model $\mathbf{r}^{(k)}$ and module $\mathbf{x}^{(k)}$, to solve the recovery problem.

Module $\mathbf{r}^{(k)}$ corresponds to Eq. (8) and generates $\mathbf{r}^{(k)}$ from the result of the $(k-1)$ -th iteration. In order to improve flexibility of the recovery network, step size ρ in Eq. (8) may be automatically adjusted according to iteration, i.e., $\rho^{(k)}$ varies for each k . Therefore, module $\mathbf{r}^{(k)}$ can be viewed as a function of $\mathbf{x}^{(k-1)}$ and \mathbf{y} , i.e.,

$$\mathbf{r}^{(k)} = g_{\Phi, \rho^{(k)}}(\mathbf{x}^{(k-1)}, \mathbf{y}) = \mathbf{x}^{(k-1)} - \rho^{(k)}\Phi^\top (\Phi\mathbf{x}^{(k-1)} - \mathbf{y}). \quad (10)$$

Module $\mathbf{x}^{(k)}$ corresponds to Eq. (9) and calculates $\mathbf{x}^{(k)}$ from $\mathbf{r}^{(k)}$ in the k -th iteration. A combination of two convolutional layers and a ReLU unit (i.e. a diode) $\text{ReLU}(x) = \max(0, x)$ is used to construct the sparse transformation $\mathcal{F}(\cdot)$ in Eq. (9), i.e., $\mathcal{F}(\mathbf{x}) = \mathbf{B} \cdot \text{ReLU}(\mathbf{A}\mathbf{x})$. Both \mathbf{A} and \mathbf{B} use convolutional layers without bias to achieve equivalent matrix operations. To overcome the vanishing gradient issue which often leads to poorer performance in deep unfolding, a residual structure is constructed to enhance recovery accuracy.

From Eq. (9), we assume that $\mathbf{x}^{(k)} = \mathbf{r}^{(k)} + \mathbf{w}^{(k)} + \mathbf{e}^{(k)}$, where $\mathbf{w}^{(k)}$ represents the missing high-frequency components in $\mathbf{r}^{(k)}$, and $\mathbf{e}^{(k)}$ denotes noise. We then apply a linear operation $\mathcal{R}(\cdot)$ to extract missing component $\mathbf{w}^{(k)}$ from $\mathbf{x}^{(k)}$, i.e., $\mathbf{w}^{(k)} = \mathcal{R}(\mathbf{x}^{(k)})$. Define $\mathcal{R}(\cdot)$ as $\mathcal{R} = \mathcal{B} \circ \mathcal{M}$, where \mathcal{M} and \mathcal{B} corresponds to a convolutional layer without bias terms with kernel size 3×3 . Note that when a sparse transformation satisfies $\mathcal{F}(\mathbf{x}) = \mathbf{BReLU}(\mathbf{A}\mathbf{x})$, the following approximation holds: $\|\mathcal{F}(\mathbf{x}) - \mathcal{F}(\mathbf{r}^{(k)})\|^2 \approx \alpha \|\mathbf{x} - \mathbf{r}^{(k)}\|^2$ [21], where α is a scalar only related to parameters of transformation $\mathcal{F}(\cdot)$. Next, decompose $\mathcal{F}^{(k)}$ into $\mathcal{F}^{(k)} = \mathcal{H}^{(k)} \circ \mathcal{M}^{(k)}$, where $\mathcal{H}^{(k)}$ consists of two convolutional layers without bias plus a ReLU activation. Eq. (9) can be transformed into

$$\begin{aligned} \mathbf{x}^{(k)} = \operatorname{argmin}_{\mathbf{x}} & \frac{1}{2} \left\| \mathcal{H}^{(k)}(\mathcal{M}^{(k)}(\mathbf{x})) - \mathcal{H}^{(k)}(\mathcal{M}^{(k)}(\mathbf{r}^{(k)})) \right\|^2 \\ & + \theta^{(k)} \|\mathcal{H}^{(k)}(\mathcal{M}^{(k)}(\mathbf{x}))\|_1. \end{aligned} \quad (11)$$

Next, construct the left inverse function of $\mathcal{H}^{(k)}(\cdot)$ such that $\tilde{\mathcal{H}}^{(k)} \circ \mathcal{H}^{(k)} = \mathcal{I}$, where \mathcal{I} is the identity operator. We then can use a DNN to construct a symmetric structure of $\tilde{\mathcal{H}}^{(k)}(\cdot)$ as $\mathcal{H}^{(k)}(\cdot)$, and include the constraint of $\tilde{\mathcal{H}}^{(k)} \circ \mathcal{H}^{(k)} = \mathcal{I}$ to the loss function. Finally, a closed-form expression of $\mathbf{x}^{(k)}$ can be

$$\mathbf{x}^{(k)} = \mathbf{r}^{(k)} + \mathcal{B}^{(k)} \left[\tilde{\mathcal{H}}^{(k)} \left[\operatorname{soft} \left[\mathcal{H}^{(k)}(\mathcal{M}^{(k)}(\mathbf{r}^{(k)})), \theta^{(k)} \right] \right] \right], \quad (12)$$

where we define a soft threshold function $\operatorname{soft}(x, \theta) = \operatorname{sgn}(x) \max(0, |x| - \theta)$. The network structure corresponding to module $\mathbf{x}^{(k)}$ is shown in the gray box at Fig. 2. Kernel number C is set to 32 by default.

To optimize parameters in SPTM2-ISTANet+, we need an efficient loss function for training. Define the size and the n -th CSI vector of the training set, respectively, as N_T and $\mathbf{x}_n \in \mathbb{R}^N$. Define the number of iteration modules as N_I . We can construct loss function

$$\mathcal{L}_{\text{total}}(\Theta) = \mathcal{L}_{\text{MSE}} + \gamma \cdot \mathcal{L}_{\text{constraint}}, \quad (13)$$

where the mean square error (MSE) $\mathcal{L}_{\text{MSE}} = \frac{1}{N_T N} \sum_{n=1}^{N_T} \left\| \mathbf{x}_n^{(N_I)} - \mathbf{x}_n \right\|^2$ is the CSI reconstruction accuracy indicator, which is commonly used in the CSI feedback. Additionally, $\mathcal{L}_{\text{constraint}} = \frac{1}{N_T N} \sum_{n=1}^{N_T} \sum_{k=1}^{N_I} \left\| \tilde{\mathcal{H}}^{(k)} \left(\mathcal{H}^{(k)} \left(\mathcal{M}^{(k)} \left(\mathbf{r}_n^{(k)} \right) \right) \right) - \mathcal{M}^{(k)} \left(\mathbf{r}_n^{(k)} \right) \right\|^2$ corresponds to $\tilde{\mathcal{H}}^{(k)} \circ \mathcal{H}^{(k)} = \mathcal{I}$ restriction, with which γ is the regularization weight (set to 0.01 unless noted otherwise).

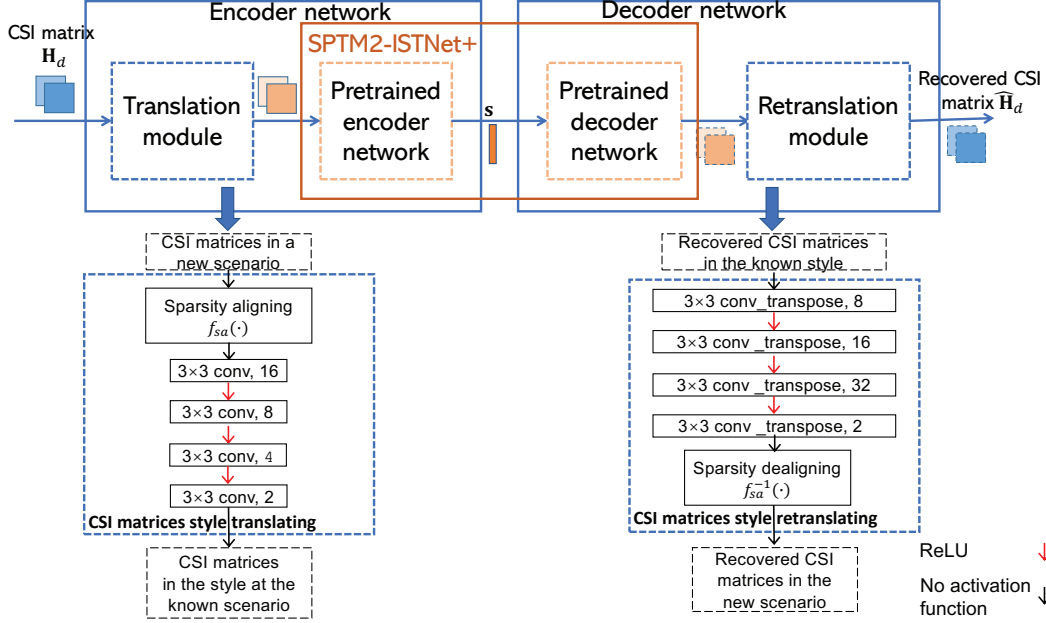


Fig. 3: Architecture of CSI-TransNet.

V. CSI TRANSLATION ARCHITECTURE CSI-TRANSNET

Tackling CSIs from various environments is one of the key challenges in the practical deployment of DL-based CSI feedback schemes. One solution is to train a customized network for each scenario or region, and dynamically switch to the feedback network according to UE-detected channel environments. However, this solution requires UE to have sufficient memory to save many DL-based encoder networks, each of which may include millions of parameters. Alternatively, UE may frequently update its encoder by downloading new model parameters, thereby consuming high cost in terms of wireless bandwidth and UE energy.

Image-to-image translation [23] has been used in computer vision to handle a variety of problems including image stylization [24] and segmentation [25]. It aims to learn a mapping that can convert an image from a source domain to a target domain, while preserving the main presentations of input images. For example, a horse image can be converted to an image similar to the zebra’s style. Motivated by the application of image-to-image translation, we propose to translate the style of CSI in a new scenario to match the style in the known scenario of a given CSI feedback model. In this section, we propose an efficient CSI feedback architecture “CSI-TransNet”, which incorporates a lightweight module on the UE side to overcome performance obstacles of DL-based CSI model in various environments. By exploiting the CSI-to-CSI

translation, CSI-TransNet can reuse the pretrained CSI model with high recovery accuracy in a new environment.

The full CSI-TransNet architecture is shown in Fig. 3, where the encoder network at UE is equipped with one translation module and one shared pretrained encoder network. The decoder network at gNB contains a shared pretrained decoder network and one customized retranslation module. Note that, the translation and retranslation modules are two plug-in modules that only need a few thousand parameters that can be easily updated each time when a UE encounters a new channel environment.

CSI-to-CSI translation makes it easier for CSI matrices after translation to be efficiently compressed and accurately recovered by the pretrained model without further tuning. Consequently, CSI matrices after translation should have a similar property to that of CSI matrices in the anchor scenario. Unlike data-based translation, as shown in Fig. 3, we customize an effective sparsity aligning function before the DL-based translation network in the translation module to achieve lightweight simplicity.

Since the CSI matrices are sparse in angular-delay domain [3], we apply circular shift in angular-delay domain to CSI matrices in a new scenario to promote a similar sparsity to the anchor scenario used to pre-train the anchor model. Define the sparsity aligning function as $f_{sa}(\cdot)$, and define the circular shift function as $f_{sh}(\cdot, i, j)$, where i and j are shift steps in row and column, respectively. For a given CSI matrix \mathbf{H} , elements of CSI matrix after the circular shift $\mathbf{H}^{sh} = f_{sh}(\mathbf{H}, i, j)$ can be written as

$$\mathbf{H}_{m,n}^{sh} = \mathbf{H}_{(m-i) \bmod R_d, (n-j) \bmod N_b}, \forall m \in [R_d], n \in [N_b]. \quad (14)$$

Consequently, the goal of the sparsity aligning function is to find shift steps i and j to achieve the best similarity. One way to achieve this goal is to calculate the shift step corresponding to the best circular cross-correlation [26] for CSI magnitude matrices from the two scenarios. A more strict and convenient way is to calculate the shifting steps i and j corresponding to the best CSI recovery accuracy of the pretrained CSI feedback network, i.e.,

$$\min_{i,j} \sum_n \|f_{sh}(\mathbf{H}_n, i, j) - f_{de,1}(f_{en,1}(f_{sh}(\mathbf{H}_n, i, j); \Phi_1); \Psi_1)\|^2 \quad (15)$$

where \mathbf{H}_n corresponds to the n -th measured CSI matrix in the new channel scenario. Owing to the translation invariance of the convolutional layers, we propose to use the second method of

(15) to determine the shift steps i and j . Given a pair of selected shift steps i and j , we can get the CSI matrix after sparsity aligning in the scenario t as

$$\mathbf{H}^{\text{sa}} = f_{\text{sa}}(\mathbf{H}^t) = f_{\text{sh}}(\mathbf{H}^t, i, j). \quad (16)$$

After sparsity aligning, DNN of the translation module consists of 4 convolutional layers for feature extraction and translation. Specifically, 4 convolutional layers utilize 3×3 kernel to generate 16, 8, 4 and 2 feature maps, respectively. The first 3 convolutional layers use the ReLU activation function.

The retranslation module mirrors the structure of the translation module, where a DL network is constructed first to fine-tune the CSI matrix, followed by a sparsity dealigning function $f_{\text{sa}}^{-1}(\cdot)$ to restore sparsity in the new scenario. To reverse convolution, transposed convolution layers [27] are used in the retranslation module. Specifically, 4 transposed convolutional layers utilize 3×3 kernel to generate 32, 16, 8 and 2 feature maps, respectively. The first 3 transposed convolutional layers use ReLU activation function. Using the same shifts steps i and j from sparsity aligning, we recover the CSI matrix in the scenario t as

$$\hat{\mathbf{H}}^t = f_{\text{sa}}^{-1}(\hat{\mathbf{H}}^{\text{sa}}) = f_{\text{sh}}(\hat{\mathbf{H}}^{\text{sa}}, -i, -j). \quad (17)$$

Let Θ_t and Ω_t be DNN parameters in the translation module and retranslation module, respectively. We write translation function $f_{\text{tra}}(\cdot; \Theta_t)$ and retranslation function $f_{\text{ret}}(\cdot; \Omega_t)$. For CSI-TransNet in the scenario t , after determining the shift steps i and j , we jointly train only parameters in the plug-in modules $f_{\text{tra}}(\cdot; \Theta_t)$ and $f_{\text{ret}}(\cdot; \Omega_t)$ using the following loss function \mathcal{L}_{MSE} :

$$\frac{1}{N_t} \sum_n \|\mathbf{H}_n^{\text{sa}} - f_{\text{det},t}(f_{\text{de},1}(f_{\text{en},1}(f_{\text{tra},t}(\mathbf{H}_n^{\text{sa}}; \Theta_t); \Phi_1); \Psi_1); \Omega_t)\|^2,$$

where N_t is the number of training CSI data samples for the t -th scenario.

When a UE detects and reports a new scenario, the gNB serving this area in the CSI-TransNet architecture sends weights of the translation module to the UE to ensure CSI feedback accuracy. In view of the lightweight design, only a few thousand parameters are included, which significantly lightens the payload in comparison with the total number of encoder parameters.

VI. MODEL-DRIVEN DATA AUGMENTATION

In addition to lowering the deployment cost of CSI feedback models in variational environments, we also consider the challenge of training DL models for CSI feedback which uses at

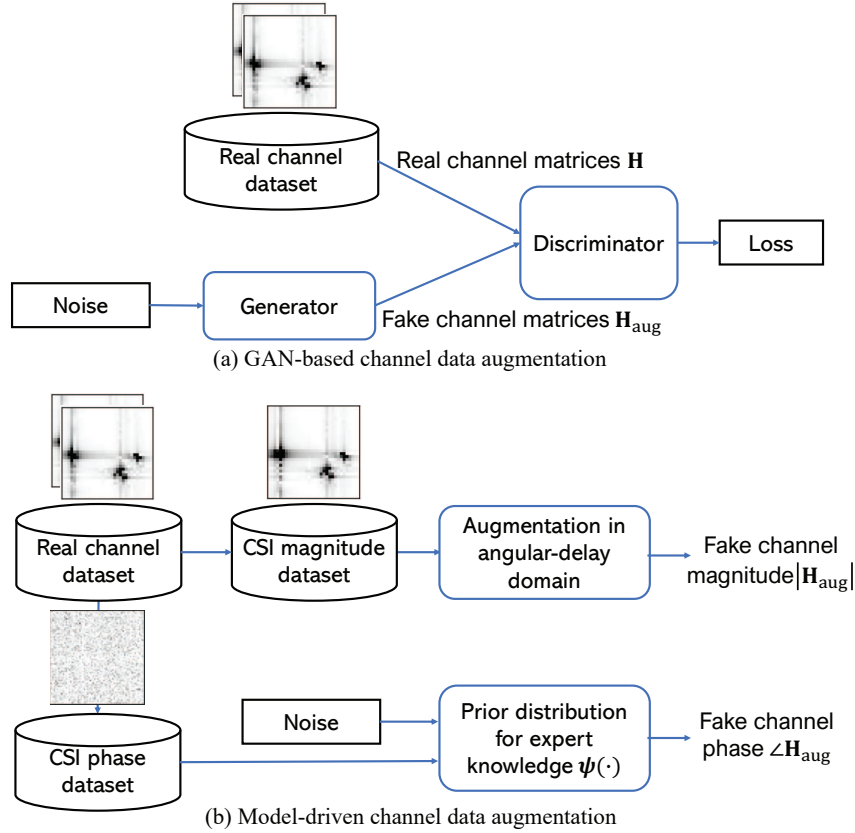


Fig. 4: Architecture comparison between proposed data augmentation and GAN-base data augmentation.

least tens of thousands of real-time channel measurements in each scenario. Many DL models have adopted data augmentation as an effective solution. We investigate how to leverage domain knowledge for data augmentation in compressive CSI feedback and recovery.

A. GAN-based Augmentation

Fig. 4(a) shows a traditional GAN-based approach to data augmentation that alternately solves maximizing and minimizing optimization problems during training to reduce the distance between the distributions of generated channels and real channels. The generator uses a DNN to map the Gaussian noise vector to generate imitations (fake channels). When GAN converges to generate channels with matching distribution to true channels, we can treat the GAN as a stable storage of CSI models for providing augmented channel data to form a large training dataset to support CSI-TransNet training. However, GAN itself requires sufficient data samples to train. Furthermore,

when available CSI measurement samples only partially represent RF channel features in a coverage area, even a well-trained generator can be a heavily biased channel model which can severely degrade the performance of compressive CSI models trained with biased CSI data. In short, it is not enough to obtain sufficient data samples in GAN-based training. It is vital for augmented samples to cover features that are absent from existing measurement samples.

B. Model-driven Augmentation

To enhance DNN training for CSI feedback, we note that augmented samples should present absent or under-represented features among existing measurements. Leveraging domain knowledge, we develop a simple but effective model-driven augmentation by decoupling the characteristics in the magnitude and phase of CSI matrices.

We begin by first split phase and magnitude of MIMO channel matrices before augmentation:

$$\mathbf{H} = |\mathbf{H}| \odot e^{j\angle\mathbf{H}}, \quad (18)$$

where \odot denotes Hadamard product. The (m, n) -th entry of \mathbf{H} is written as $\mathbf{H}_{m,n} = |\mathbf{H}_{m,n}| e^{j\angle\mathbf{H}_{m,n}}$. This way, the magnitude CSI matrix is $|\mathbf{H}|$ with entries $|\mathbf{H}_{m,n}|$ and the phase matrix is written as $\angle\mathbf{H}$ with entries $\angle\mathbf{H}_{m,n}$. This split allows us to apply domain knowledge about CSI features including multipath delay profile and phase distribution.

Next, we utilize the geographical continuity of CSI variation to generate augmented magnitude matrices, which should exhibit similar characteristics to measured channels. Given a typical environment with fixed paths between gNB and UE, it has been noted that geographically continuous UE movement should lead to smooth variation in the angular-delay domain [28]. In other words, CSIs in the vicinity of a measurement spot are highly correlated in the angular-delay domain because of similar arrival/departure angles and delays of multipath propagation. Consequently, we can construct multiple angle-delay profiles by (circularly) shifting the CSI magnitude matrix in angular-delay domain to generate new CSI matrices that reflect features of nearby UE CSIs. Leveraging the circular characteristic of CSI matrices in the angular-delay domain based on the property of DFT, the shifts are circular. In short, entries of the augmented magnitude CSI matrix $|\mathbf{H}_{m,n}^{\text{aug}}|$ are generated by the following rule in the angular-delay domain,

$$|\mathbf{H}_{m,n}^{\text{aug}}| = \begin{cases} |\mathbf{H}_{m+i,(n+j) \bmod N_b}|, & 1 \leq m+i \leq R_d, \\ 0, & \text{else,} \end{cases} \quad (19)$$

$\forall m \in [R_d], n \in [N_b]$. Note that we select shift steps $[-\frac{R_d}{2}] \leq i \leq [\frac{R_d}{2}]$ and $[-\frac{N_b}{2}] \leq j \leq [\frac{N_b}{2}]$ in angular and delay domain, respectively. We apply truncation in the delay domain by setting to zero delay elements beyond R_d rows.

We also augment the phase matrices. The augmented phases should cover cases beyond the measured CSIs to enhance training and avoid overfitting. Considering that the path to antenna array arrived at the same delay can share frequency-independent phase shift that includes direct or reflected path [29], we select uniform distribution as augmented phase shifting distribution $\psi_{\text{aug}}(\cdot) \sim \mathcal{U}(0, 2\pi)$ to elements in the same row (i.e., same delay). In other words, we construct a larger phase variation than the measured CSI phase, and we use recall to replace some precision to enhance CSI recovery accuracy in the practical deployment. Accordingly, for each row of a sampled CSI matrix, we apply a random phase shift:

$$\angle \mathbf{H}_{m,n}^{\text{aug}} = \angle \mathbf{H}_{m,n} + \angle e^{-j\theta_m}, \forall m \in [R_d], n \in [N_b], \quad (20)$$

where $\theta_m \sim \mathcal{U}(0, 2\pi)$.

Finally, we combine augmented magnitude and phase matrices to generate CSI samples for training CSI feedback models.

VII. PERFORMANCE EVALUATION

A. Experiment Setup

For performance evaluation, we use the following four datasets, where the first two dataset settings are typically used for assessing the performance of CSI estimation and feedback techniques [3], the third dataset is from actual field measurements, and the last dataset is generated following 3GPP standard models:

- 1) **Cost2100 Indoor.** The dataset is generated by using COST2100 model [30] with 5.3 GHz downlink frequency for a gNB at the center of a 20m×20m coverage area. The bandwidth is 20 MHz. We consider $N_b = 32$ antennas and $N_f = 1024$ subcarriers at the gNB to serve single-antenna UEs randomly distributed within the coverage area.
- 2) **Cost2100 Outdoor.** The dataset is generated from COST2100 model [30] for a 300 MHz downlink frequency for a gNB at the center of a 400m×400m coverage area. The bandwidth, antennas and subcarriers are the same as in Cost2100 Indoor.
- 3) **Measured Indoor.** This dataset contains CSI samples recorded from KU Leuven Massive MIMO testbed in a 9 m² indoor area [31]. The gNB is equipped with a Uniform Linear

Array (ULA) of 64 antennas. We select the middle 32 of 64 antennas. The CSI is collected for 100 subcarriers spaced at a 2.61 GHz frequency over a 20 MHz bandwidth.

- 4) **Quadriga 3GPP UMA.** We generate one more dataset using the channel setting described in 3GPP TR 38.901 with the QuaDRiGa platform [32]. We select the urban macrocell (UMa) scenario at the 2.6 GHz carrier. We consider gNB with $N_b = 32$ antennas and $N_f = 1024$ subcarriers over 20 MHz bandwidth. The gNB is located at the center of a square area of edge length 400m and serves single-antenna UEs randomly distributed within the coverage area.

After transforming CSI matrices into the angular-delay domain, only the first 32 rows are kept owing to sparsity for these four types of channel data. The overall training set size is 100,000 and the testing set size is 20,000. The batch size is 64. We use 200 epochs for SPTM2-ISTANet+, and 80 epochs for the translation module and retranslation module in CSI-TransNet because they have very few parameters.

To compare the recovery accuracy of different networks, we adopt the metric of normalized MSE, i.e., $\text{NMSE} = \frac{1}{N_k} \sum_{k=1}^{N_k} \|\mathbf{H}_k - \hat{\mathbf{H}}_k\|^2 / \|\mathbf{H}_k\|^2$, where $\hat{\mathbf{H}}$ is the recovered \mathbf{H} , k and N_k are the index and the number of samples in the testing set, respectively.

B. Feedback Accuracy Comparison of the Anchor Model

We compare SPTM2-ISTANet+ with three known schemes with demonstrated performance in massive MIMO system CSI feedback (without relying on additional auxiliary information, e.g., uplink CSI, previous CSIs):

- CsiNet+ [5]: A CSI feedback model that uses larger convolution kernels (7×7) and optimizes the structure of residual units.
- DCRNet [6]: A modified CRNet [4] that combines multiple resolution convolution kernels and dilated convolutions to extract CSI features of the different granularities. It optimizes learning rate adjustment with the help of a warm-up process.
- ISTANet+: A design inspired by compressive image processing [21] for CSI feedback in [12] which adopts orthogonal random Gaussian measurement matrix $\Phi \in \mathbb{R}^{M \times N}$, where $N = 2048$, M depends on CR.

Furthermore, we consider one more method TM2-ISTANet+, which is the SPTM2-ISTANet+ without spherical processing, to showcase the advantage of different components in SPTM2-ISTANet+.

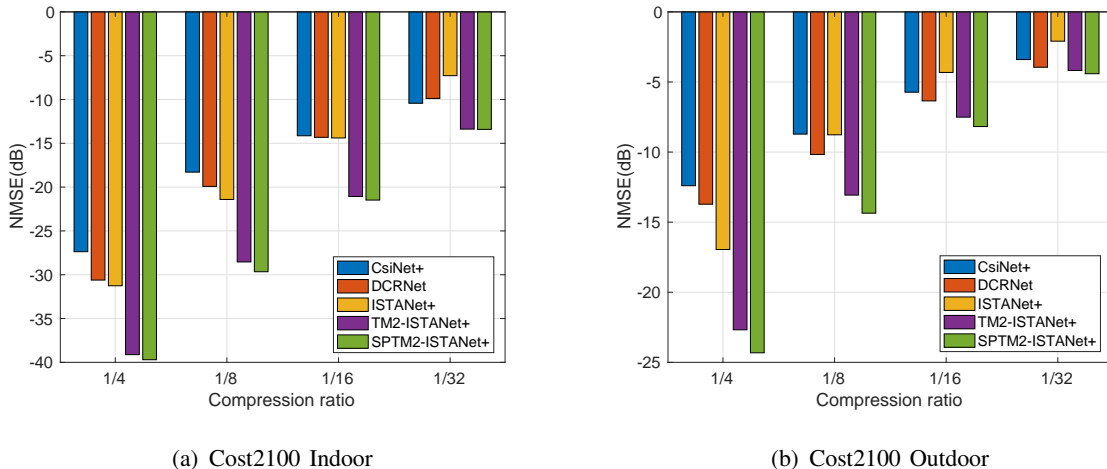


Fig. 5: NMSE comparison in different CRs.

Fig. 5 shows the CSI performance comparison among the five schemes CsiNet+, DCRNet, ISTANet+, TM2-ISTANet+ and SPTM2-ISTANet+ at different CRs for indoor and outdoor scenarios using the Cost2100 model. These two datasets are commonly used in the CSI feedback works [4], [5], [6], [7]. The number of iteration blocks is set to 9. As shown in Fig. 5(a)(b), our proposed SPTM2-ISTANet+ can achieve superior performance at all tested CRs. In particular, for CR of 1/4 in the challenging outdoor scenario, SPTM2-ISTANet+ provides approximately 10dB improvement in CSI reconstruction accuracy compared to traditional DL-based schemes DCRNet and CsiNet+. On the other hand, we notice that ISTANet+ performs better than CsiNet+ and DCRNet for larger CR (such as 1/4). The performance of ISTANet+ is worse than that of CsiNet+ and DCRNet at the higher compression (i.e. smaller CR), e.g., 1/32. Our test results show that the random measurement matrix Φ from traditional CS methods does not effectively extract key data features for small CR values. On the other hand, TM2-ISTANet+ based on the data-driven measurement matrix performs better. Moreover, we also note the advantages of SPTM2-ISTANet+ that are attributable to spherical processing for all tested CR values.

Fig. 6 shows the impact of the number of iteration blocks N_I on the CSI feedback performance of ISTANet+, TM2-ISTANet+ and SPTM2-ISTANet+ when CR= 1/4 in indoor and outdoor scenarios against Cost2100 channel model. We observe that SPTM2-ISTANet+ delivers the best performance at various iterations. In fact, with only 3 iterations, it achieves similar performance to ISTANet+ using 12-iterations. Evidently, the performance of SPTM2-ISTANet+ stabilizes after the number of iterative modules reaches 9. Actually, 3 iteration modules would suffice for indoor channels at CR = 1/4 since NMSE has already fallen below -30 dB, whereas 9 iterations

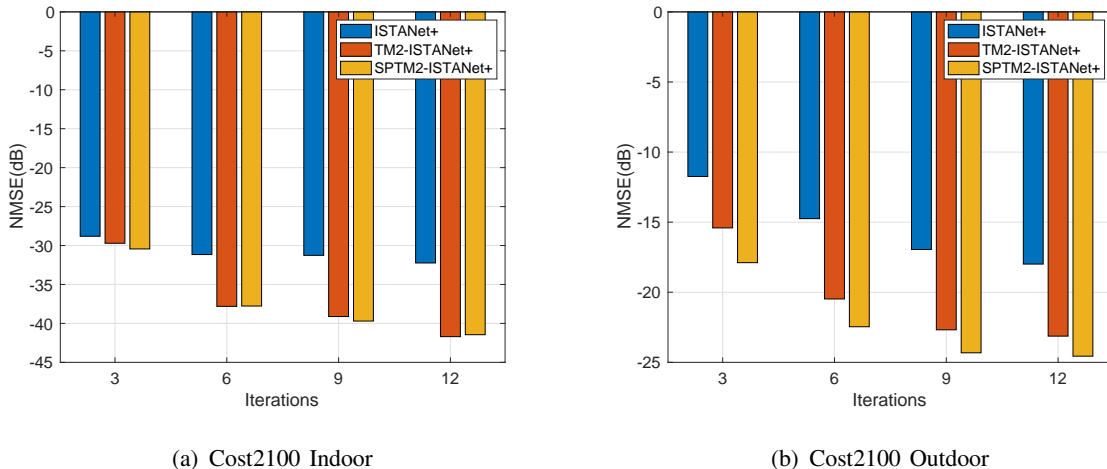


Fig. 6: NMSE at different iteration blocks for $CR = 1/4$.

would suffice for outdoor channels. The underlying reason is that channels and CSI variations in outdoor cases are relatively complex. Hence, more iterative modules are needed.

C. Data Augmentation Comparison

Since DL-based CSI feedback works have already achieved satisfactory performance for the indoor scenario [4], [5], [6], [7], we focus on the outdoor scenario where practical CSI measurement is even harder and CSI recovery is less accurate. For data augmentation, samples from the limited measurements will be randomly selected from the training set in Cost2100 Outdoor. We set shift ranges in the angular domain and delay domain to -15 to 15 and -3 to 3 , respectively. We set the training dataset size after augmentation to the same overall training set size by repetition or phase randomization if the initial augmentation is not large enough (depending on the corresponding augmentation method).

Fig. 7 compares the performance of SPTM2-ISTANet+ using different augmentation strategies including the costly blackbox “ChannelGAN” [16], no augmentation (“No Aug”) which uses repetition to enlarge dataset size, shift in angular-delay domain (“ADS”) where repetition is used to enlarge dataset size only if necessary, random phase shift (“PRS”), and ADS together with PRS (ADS+PRS). We set the $CR = 1/4$. We limit the number of CSI measurements before augmentation to 100, 200, 500, and 1000, respectively. As shown in Fig. 7, our proposed ADS and ADS+PRS significantly outperform ChannelGAN in each case. In fact, PRS alone already outperforms ChannelGAN. Notably, ADS+PRS can achieve NMSE of -15.8 dB using only 100

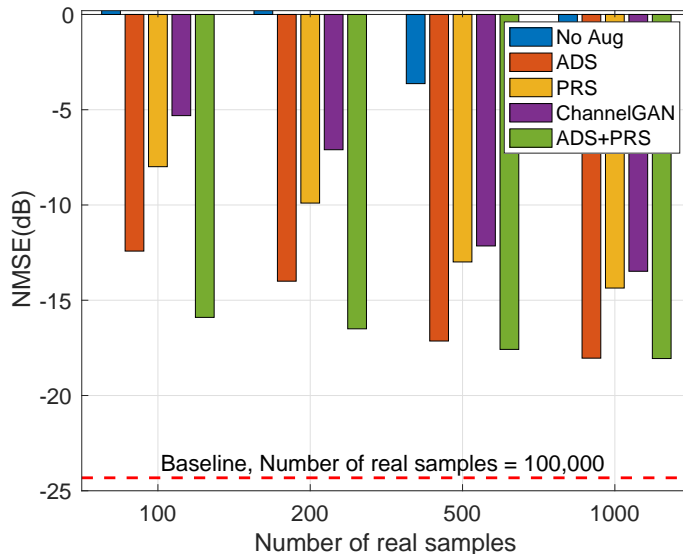


Fig. 7: Augmentation comparison at CR = 1/4.

CSI measurement samples whereas ChannelGAN reaches -5.3 dB. Furthermore, both ADS and PRS improve CSI recovery accuracy. Overall, the proposed low-cost training enhancement by using ADS always achieves higher gains than PRS owing to the better utilization of geographical correlation based on domain knowledge.

D. Recovery Comparison against New Scenarios

To evaluate recovery performance when UE encounters a new scenario, we select the model pretrained from Cost2100 Indoor, Cost2100 Outdoor, Measured Indoor and Quadriga 3GPP UMA, respectively. For each model, we use the other three datasets unseen by the pretrained model as new scenarios.

Fig. 8 shows CSI feedback performance for the model pretrained in one scenario to the new scenarios at CR = 1/4. “SPTM2-ISTANet+, Direct” denotes the performance of the pretrained SPTM2-ISTANet+ in the new scenario without preprocessing, “SPTM2-ISTANet+, SpaAlign” shows the performance of the pretrained SPTM2-ISTANet+ with the help of the sparsity aligning function $f_{sa}(\cdot)$, “CSI-TransNet, Aug200” indicates the performance of CSI-TransNet with the help of the proposed ADS+PRS augmentation starting with 200 samples from the new scenario. As baselines, “CSI-TransNet, Full” corresponds to CSI-TransNet trained with the full training sets in the new scenario, and “SPTM2-ISTANet+, Retrained” corresponds to the performance of SPTM2-ISTANet+ that are retrained from scratch in the new scenario.

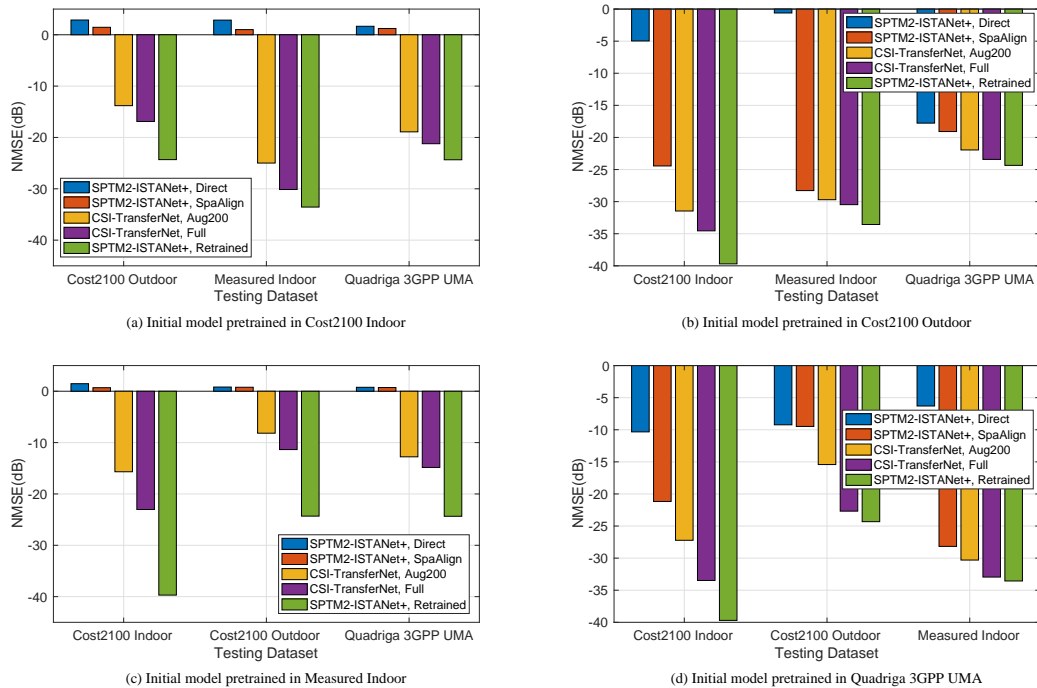


Fig. 8: CSI feedback performance comparison for the model pretrained in one scenario to the new scenarios when $CR = 1/4$.

As shown in Fig. 8, “SPTM2-ISTANet+, Direct” generally suffers poor CSI recovery accuracy, which is consistent with common knowledge that DL-based CSI feedback has limited ability to handle more general CSIs. With the help of sparsity aligning, the models pretrained on Cost2100 Outdoor and Quadriga 3GPP UMA demonstrate clear accuracy improvement in the new scenarios, while the models pretrained on Cost2100 Indoor and Measured Indoor do not. Actually, compared with Cost2100 Indoor and Measured Indoor, CSI in Cost2100 Outdoor and Quadriga 3GPP UMA exhibit more diverse features in terms of multipath delay and angle of arrival/departure distributions. This allows models pretrained in more diverse environments to tackle more general channel scenarios.

With limited measurement data, “CSI-TransNet, Aug200” illustrates obvious performance improvement for each case, especially for the anchor model pretrained on Cost2100 Indoor and Measured Indoor. This observation confirms the effectiveness of our proposed plug-in translation module and model-driven channel data augmentation. “CSI-TransNet, Full” provides additional gains over “CSI-TransNet, Aug200”, which means that a more accurate CSI-to-CSI translation

can benefit more from the pretrained model. “SPTM2-ISTANet+, Retrained” is selected as the performance bound for the CSI feedback accuracy. We observe that the models pretrained on Cost2100 Outdoor and Quadriga 3GPP UMA exhibit smaller gaps to the retraining bound. Consequently, we suggest using the model pretrained in a more diverse (complex) environment (such as outdoor) to serve as the anchor network in CSI-TransNet.

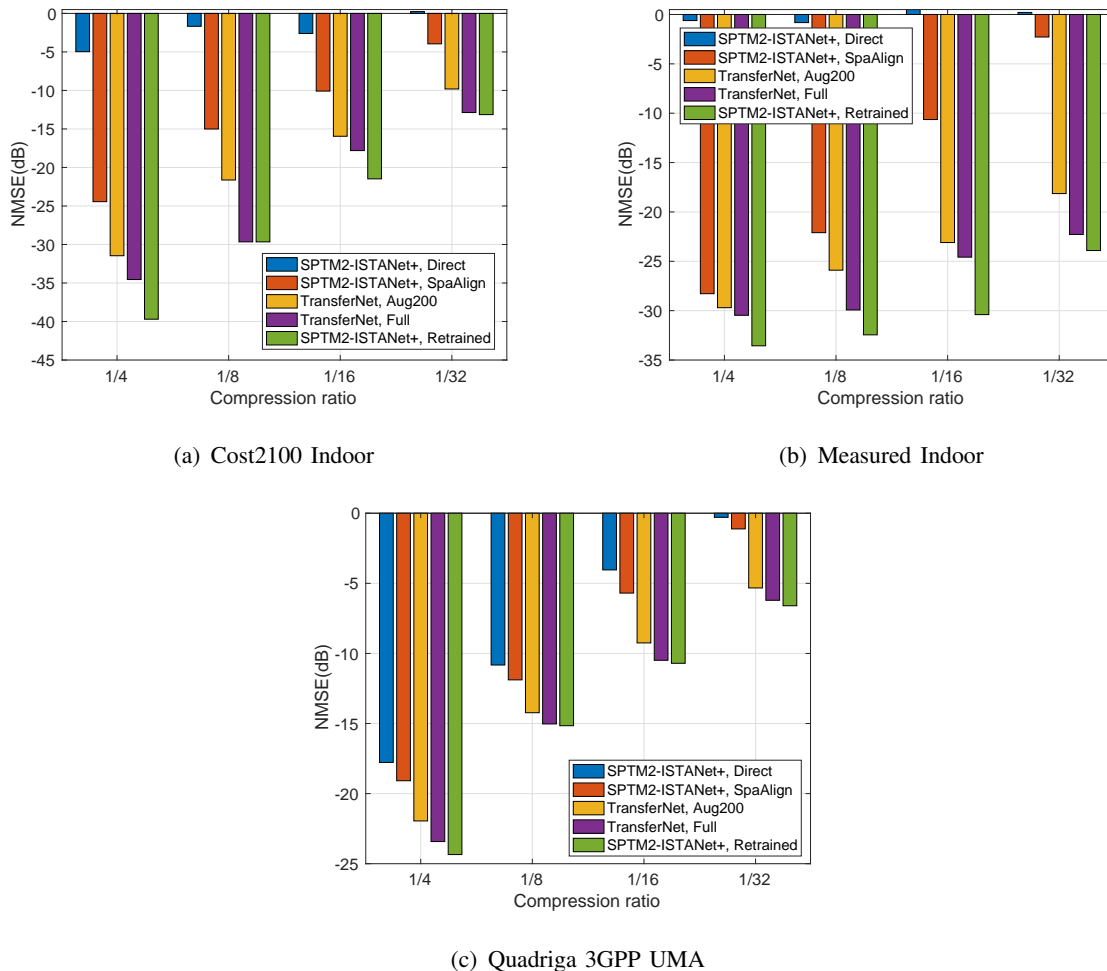


Fig. 9: CSI feedback performance comparison in different CRs for the model pretrained in the Cost2100 Outdoor dataset to the new scenarios.

We now consider the CSI recovery for different CR levels. Fig. 9 shows the performance of the model pretrained on the Cost2100 Outdoor dataset under new scenarios. We observe that “CSI-TransNet, Full” always has similar CSI recovery as “SPTM2-ISTANet+, Retrained”, which suggests that our proposed plug-in CSI-to-CSI translation design is able to reuse the pretrained

TABLE I: Model size and computational complexity of encoder networks in UE. M: million, K: thousand.

	Parameters				FLOPs			
	CsiNet+	DCRNet	SPTM2-ISTANet+	TransModule	CsiNet+	DCRNet	SPTM2-ISTANet+	TransModule
$CR=\frac{1}{4}$	1.1 M	1.0 M	1.0 M	1.8 K	2.9 M	2.6 M	2.1 M	3.7 M
$CR=\frac{1}{8}$	0.5 M	0.5 M	0.5 M	1.8 K	1.9 M	1.6 M	1.0 M	3.7 M
$CR=\frac{1}{16}$	0.3 M	0.3 M	0.3 M	1.8 K	1.3 M	1.0 M	0.5 M	3.7 M
$CR=\frac{1}{32}$	0.1 M	0.1 M	0.1 M	1.8 K	1.1 M	0.8 M	0.3 M	3.7 M

model and weights effectively. We also observe that “CSI-TransNet, Aug200” achieves NMSE accuracy below -20 dB at $CR = 1/4$ and below -9 dB at $CR = 1/16$ in other scenarios. This establishes “CSI-TransNet, Aug200” as a good anchor network and suggests that the anchor network pretrained on a diverse environment benefits scenario-adaptive design.

Interestingly, note that carrier frequencies of Cost2100 Indoor, Measured Indoor and Quadriga 3GPP UMA are different from that of Cost2100 Outdoor. In fact, the subcarrier spacing of Measured Indoor is also different from Cost2100 Outdoor. The performance robustness of CSI-TransNet irrespective of the difference in terms of carrier frequencies and subcarrier spacing shows that our proposed CSI-TransNet architecture is less rigid and can reuse pretrained networks across different scenarios. Using very limited new measurements from a new environment, CSI-TransNet reduces the cost of practical deployment in diverse and complex wireless environments.

E. Complexity Comparison

We provide some discussions with respect to algorithm complexity. Table I compares parameters and FLOPs of the cost-sensitive UE encoder. We do not find it interesting to compare decoder networks because the computation power and energy of resource-rich gNBs are generally of less concern. The comparison shows that SPTM2-ISTANet+ can reduce UE computation by over 27% and 19%, respectively, in comparison with CsiNet+ and DCRNet at $CR=1/4$. Computation saving grows as CR decreases. The size (number of parameters) of the above three encoders are at a similar level. Additionally, compared with the traditional encoder networks, our new plug-in translation module can reduce the number of UE parameters that require updating in

a new scenario from 1 million down to 1.8 thousand. Even though FLOPs of the translation module are 2 times greater at $CR=1/4$, the computation complexity can be further reduced by exploiting the principle of the lightweight optimization [33], such as depth-wise convolutional design [34] and knowledge distillation [35].

Table II compares parameters and FLOPs of different augmentation strategies. Unlike ChannelGAN which requires millions of parameters and billions of FLOPs, our proposed ADS+PRS only needs several thousand parameters and FLOPs to achieve a higher CSI recovery accuracy.

TABLE II: Parameters and computational complexity of augmentation strategies. B: Billion, M: Million, K: thousand.

	ChannelGAN	ADS	PRS	ADS+PRS
Parameters	11.7 M	0.2 K	1 K	1 K
FLOPs	5.4 B	-	4.1 K	4.1 K

VIII. CONCLUSIONS

This work develops a novel solution for training and deployment enhancement of DL models in massive MIMO CSI feedback. We consider two major obstacles to DL-based feedback frameworks: new unseen channel environments and small training datasets from field measurement. For new channel environments, we present an efficient scenario-adaptive CSI feedback architecture “CSI-TransNet”. CSI-TransNet exploits the plug-in CSI-to-CSI translation module to reuse the pretrained anchor CSI model with high recovery accuracy and enables a lightweight encoder update in new scenarios. We develop an efficient deep unfolding-based CSI feedback network SPTM2-ISTANet+ as the CSI-TransNet backbone. Against small measurement datasets, we propose a simple and effective data augmentation strategy based on domain knowledge to replace blockbox GAN-based augmentation. Our proposed augmentation strategy together with CSI-TransNet can significantly enhance CSI recovery performance with only a thousand encoder parameters for update and can achieve NMSE below -20 dB by using only 200 measurement channel samples in three new scenarios at CR of $1/4$.

ACKNOWLEDGMENT

The authors would like to acknowledge Yu-Chien Lin for his useful discussions in the process of preparing this manuscript.

REFERENCES

- [1] Z. Gao, L. Dai, Z. Wang, and S. Chen, "Spatially common sparsity based adaptive channel estimation and feedback for FDD massive MIMO," *IEEE Trans. Signal Process.*, vol. 63, no. 23, pp. 6169–6183, Dec 2015.
- [2] H. Son and Y. Cho, "Analysis of compressed CSI feedback in MISO systems," *IEEE Wireless Commun. Lett.*, vol. 8, no. 6, pp. 1671–1674, Dec 2019.
- [3] C. Wen, W. Shih, and S. Jin, "Deep Learning for Massive MIMO CSI Feedback," *IEEE Wireless Commun. Lett.*, vol. 7, no. 5, pp. 748–751, Oct 2018.
- [4] Z. Lu, J. Wang, and J. Song, "Multi-resolution CSI feedback with deep learning in massive MIMO system," in *ICC 2020 - 2020 IEEE Int. Conf. on Commun. (ICC)*, 2020, pp. 1–6.
- [5] J. Guo, C. Wen, S. Jin, and G. Y. Li, "Convolutional neural network-based multiple-rate compressive sensing for massive MIMO CSI feedback: design, simulation, and analysis," *IEEE Trans. Wireless Commun.*, vol. 19, no. 4, pp. 2827–2840, 2020.
- [6] S. Tang, J. Xia, L. Fan, X. Lei, W. Xu, and A. Nallanathan, "Dilated convolution based CSI feedback compression for massive MIMO systems," *IEEE Trans. Veh. Tech.*, pp. 1–6, 2022.
- [7] X. Chen, C. Deng, B. Zhou, H. Zhang, G. Yang, and S. Ma, "High-accuracy CSI feedback with super-resolution network for massive MIMO systems," *IEEE Wireless Commun. Letters*, vol. 11, no. 1, pp. 141–145, 2022.
- [8] Y.-C. Lin, Z. Liu, T.-S. Lee, and Z. Ding, "Deep learning phase compression for MIMO CSI feedback by exploiting FDD channel reciprocity," *IEEE Wireless Commun. Lett.*, vol. 10, no. 10, pp. 2200–2204, 2021.
- [9] J. Guo, C.-K. Wen, and S. Jin, "CANet: Uplink-aided downlink channel acquisition in FDD massive MIMO using deep learning," *IEEE Trans. Commun.*, vol. 70, no. 1, pp. 199–214, 2022.
- [10] T. Wang, C. Wen, S. Jin, and G. Y. Li, "Deep Learning-Based CSI Feedback Approach for Time-Varying Massive MIMO Channels," *IEEE Wireless Commun. Lett.*, vol. 8, no. 2, pp. 416–419, April 2019.
- [11] Z. Liu, M. del Rosario, and Z. Ding, "A Markovian model-driven deep learning framework for massive MIMO CSI feedback," *IEEE Trans. Wireless Commun.*, vol. 21, no. 2, pp. 1214–1228, 2022.
- [12] M. Del Rosario and Z. Ding, "Learning-based MIMO channel estimation under practical pilot sparsity and feedback compression," *IEEE Trans. Wireless Commun.*, pp. 1–1, 2022.
- [13] C. Shorten and T. M. Khoshgoftaar, "A survey on image data augmentation for deep learning," *Journal of Big Data*, vol. 6, no. 1, pp. 1–48, 2019.
- [14] Y. Yang, Y. Li, W. Zhang, F. Qin, P. Zhu, and C.-X. Wang, "Generative-adversarial-network-based wireless channel modeling: Challenges and opportunities," *IEEE Commun. Mag.*, vol. 57, no. 3, pp. 22–27, 2019.
- [15] H. Ye, L. Liang, G. Y. Li, and B.-H. Juang, "Deep learning-based end-to-end wireless communication systems with conditional GANs as unknown channels," *IEEE Trans. Wireless Commun.*, vol. 19, no. 5, pp. 3133–3143, 2020.
- [16] H. Xiao, W. Tian, W. Liu, and J. Shen, "ChannelGAN: Deep learning based channel modeling and generating," *IEEE Wireless Commun. Lett.*, vol. 11, no. 3, pp. 650–654, 2022.
- [17] Y. Yang, F. Gao, Z. Zhong, B. Ai, and A. Alkhateeb, "Deep transfer learning-based downlink channel prediction for FDD massive MIMO systems," *IEEE Trans. Commun.*, vol. 68, no. 12, pp. 7485–7497, 2020.

- [18] J. Zeng, J. Sun, G. Gui, B. Adebisi, T. Ohtsuki, H. Gacanin, and H. Sari, "Downlink CSI feedback algorithm with deep transfer learning for FDD massive MIMO systems," *IEEE Trans. Cogn. Commun. Netw.*, vol. 7, no. 4, pp. 1253–1265, 2021.
- [19] X. Li, J. Guo, C.-K. Wen, S. Jin, and S. Han, "Multi-task learning-based CSI feedback design in multiple scenarios," 2022. [Online]. Available: <https://arxiv.org/abs/2204.12698>
- [20] Z. Lu, J. Wang, and J. Song, "Multi-resolution CSI Feedback with Deep Learning in Massive MIMO System," in *ICC 2020 - 2020 IEEE Int. Conf. on Commun. (ICC)*, 2020, pp. 1–6.
- [21] J. Zhang and B. Ghanem, "ISTA-Net: Interpretable optimization-inspired deep network for image compressive sensing," in *2018 IEEE/CVF Conference on CVPR*, 2018, pp. 1828–1837.
- [22] A. Beck and M. Teboulle, "A fast iterative shrinkage-thresholding algorithm for linear inverse problems," *SIAM Journal on Imaging Sciences*, vol. 2, no. 1, pp. 183–202, 2009.
- [23] C. Wang, C. Xu, C. Wang, and D. Tao, "Perceptual adversarial networks for image-to-image transformation," *IEEE Trans. Image Process.*, vol. 27, no. 8, pp. 4066–4079, 2018.
- [24] T. Park, A. A. Efros, R. Zhang, and J.-Y. Zhu, "Contrastive learning for unpaired image-to-image translation," in *ECCV 2020*. Springer International Publishing, 2020, pp. 319–345.
- [25] V. Badrinarayanan, A. Kendall, and R. Cipolla, "SegNet: A deep convolutional encoder-decoder architecture for image segmentation," *IEEE Trans. Pattern Anal. Mach. Intell.*, vol. 39, no. 12, pp. 2481–2495, 2017.
- [26] C. Wang, "Kernel learning for visual perception, chapter 2.2," Ph.D. dissertation, Nanyang Technological University, 2019.
- [27] V. Dumoulin and F. Visin, "A guide to convolution arithmetic for deep learning," 2016. [Online]. Available: <https://arxiv.org/abs/1603.07285>
- [28] F. Hejazi, K. Vuckovic, and N. Rahnavard, "DyLoc: Dynamic localization for massive MIMO using predictive recurrent neural networks," in *INFOCOM 2021 - 2021 IEEE Int. Conf. on Comput. Commun. (INFOCOM)*, 2021, pp. 1–9.
- [29] D. Tse and P. Viswanath, *Fundamentals of wireless communication*. Cambridge university press, 2005.
- [30] L. Liu, C. Oestges, J. Poutanen, K. Haneda, P. Vainikainen, F. Quitin, F. Tufvesson, and P. D. Doncker, "The COST 2100 MIMO channel model," *IEEE Wireless Commun.*, vol. 19, no. 6, pp. 92–99, December 2012.
- [31] S. De Bast and S. Pollin, "Ultra dense indoor MaMIMO CSI dataset," *IEEE Dataport*, 2021. [Online]. Available: <https://dx.doi.org/10.21227/nr6k-8r78>
- [32] S. Jaeckel, L. Raschkowski, K. Börner, and L. Thiele, "Quadriga: A 3-D multi-cell channel model with time evolution for enabling virtual field trials," *IEEE Trans. Antennas and Propag.*, vol. 62, no. 6, pp. 3242–3256, 2014.
- [33] J. Guo, J. Wang, C.-K. Wen, S. Jin, and G. Y. Li, "Compression and acceleration of neural networks for communications," *IEEE Wireless Commun.*, vol. 27, no. 4, pp. 110–117, 2020.
- [34] Z. Cao, W.-T. Shih, J. Guo, C.-K. Wen, and S. Jin, "Lightweight convolutional neural networks for CSI feedback in massive MIMO," *IEEE Commun. Lett.*, vol. 25, no. 8, pp. 2624–2628, 2021.
- [35] Z. Lu, X. Zhang, R. Zeng, and J. Wang, "Better lightweight network for free: Codeword mimic learning for massive MIMO CSI feedback," 2022. [Online]. Available: <https://arxiv.org/abs/2210.16544>